Supporting Information

Allentoft et al. 10.1073/pnas.1314972111

SI Materials and Methods

STRUCTURE Analyses. First, all four species were analyzed together to assess whether these atypical heterochronous microsatellite data contained a genetic signal at the most basic level. If STRUCTURE could not separate the four species into distinct clusters, the data would not be suitable to infer more subtle intraspecific patterns. The analysis was run by assuming four, five, and six genetic groups, respectively (K = 4, 5, 6), and each run was repeated twice to ensure consistency. Default settings were applied, allowing for genetic admixture and correlated allele frequencies. Both circumstances are somewhat unlikely given that the combined dataset represents four different species. However, because this initial analysis was conducted to illuminate the power of resolution with these microsatellite data rather than being biologically correct, the same priors were chosen as would be applied in the subsequent intraspecific assessments. The Markov chain Monte Carlo (MCMC) was run for 10^6 iterations and a burn-in of 10^4 states. The result is shown in Fig. S2.

To investigate intraspecific genetic structure, microsatellite data from each taxon were run separately at K = 1, 2, 3, with the same settings as outlined above.

Lastly, data from the 10 oldest and 10 youngest individuals were pooled in each species, respectively, and run for K = 2 under the same settings as above, to investigate whether shifts in allele frequencies had happened during the intervening time period. For *Dinornis robustus*, for example, the two temporal groups covered 4837–3270 B.P. and 602–1043 B.P., respectively, leaving a 2,200-y gap for genetic changes to have occurred. See resulting example in Fig. S2.

BEAST Analyses. To maintain chronological accuracy of the coalescent events in the genealogy, only sequences with associated radiocarbon dates were included in this analysis. A relaxed molecular clock was applied with a prior mutation rate of 8.7×10^{-8} per site per year, which represent a cross-species estimate of mutation rate for mtDNA in moa (1). The mutation rate was incorporated as a mean value in a normal distribution (SD = 0.0005). The prior value for effective population size ($N_e \times$ generation time) was set to 10^3 with a uniform distribution of 100 to 10^6. This value can be considered a broad prior, but this was necessary to cover previous estimates of moa population sizes (2, 3). Ten sampling groups were used to smooth the Bayesian skyline plot (BSP). Initial test runs evaluated in TRACER (Version 1.5; ref. 4) indicated that long MCMC runs were necessary to reach chain convergence and effective sample sizes (ESSs) >200, as recommended by the authors (5, 6). Hence, for the full analyses, the MCMC was set to generate 10^8 trees, sampled every 10^4 states. The BSP analysis for *Emeus crassus*, *Pachyornis elephantopus*, and *Euryapteryx curtus* resulted in signals with extremely large highest posterior densities (HPDs) and were therefore not evaluated further. Small datasets (fewer associated radiocarbon dates) and/or too little genetic variability to model genealogy was likely to be responsible for the inconclusive signals. The *D. robustus* data generated a more robust signal (Fig. 3) and was investigated further:

First, many independent Bayesian evolutionary analysis by sampling trees (BEAST) runs, using a range of different prior settings, were conducted; they all yielded BSP signals very similar to that shown in Fig. 3. Incorporation of an age-dependent DNA damage model, appropriate for some ancient DNA data (7), introduction of 50-y error margins on each individual radiocarbon age, or using a GTR+I+G substitution model did not affect the BSP signal. Switching to a strict molecular clock had a marginal effect, in that it narrowed the HPDs slightly and increased the (mean) time to the root of the tree. In total, these analyses confirmed that the recorded BSP signal for the *Dinornis* data was not an artifact of the chosen model.

Next, BEAST was run from an empty alignment. By applying the same user-defined model and prior settings, but excluding the DNA sequences, it was possible to test whether the BSP signal was driven by the genetic information or if it was simply an effect of prior settings (6). The output from that run showed very small ESS values and a BSP signal that did not resemble the previous runs. These results further indicated that the original BSP signal observed for *Dinornis* (Fig. 3) was not an artifact of the user-defined models and priors.

In addition to the BSP runs, we performed more restricted BEAST analyses in which a single change point from a constant to an exponentially declining/expanding population was modeled. We used two complementary approaches [similar to the free model and the model selection approaches in the approximate Bayesian computation (ABC) analyses; see below]: in one approach, the growth rate was allowed to vary between positive and negative values, and in the other approach, we restricted it to be either positive or negative (see Table S3 for prior values). We then assessed the respective posterior probabilities of these demographic models and estimated the posterior density of the relevant parameters.

ABC Analyses. In all scenarios, transitions from a constant population size at some time in the past were modeled to avoid monotonically increasing or decreasing population sizes; both are biologically unrealistic, and the latter is computationally intractable because of unrealistically high ancestral population size estimates. For each scenario, we performed 1 million simulation steps with demographic parameter values drawn from log uniform prior distributions (Table 3) using the software ABCtoolbox (8). We simulated samples with time points corresponding to the ages of the 74 *D. robustus* individuals for which we had both mtDNA and microsatellite data. Because there was no obvious sample partition or a before-and-after scenario to test, we simply partitioned the datasets into two age bins with equal sample representation (n = 37). This approach allowed us to compute a total of 19 summary statistics (Table S5) both within and across age bins using both mtDNA and microsatellite data. The numbers simulated under the three different demographic scenarios were then compared to the summary statistics from the observed datasets by using ABC (9).

Changing the binning of samples so that the two bins corresponded to equal time intervals (one bin containing 16 samples older than 2720 B.P., and the other bin included 58 samples younger than 2720 B.P.) instead of equal bin sizes had an insignificant impact on estimated parameter values and no effect on the model choice. The same was true for exploratory analyses with five age bins rather than two. We therefore conclude that the ABC results are robust to the binning scheme.

We used ABCtoolbox to perform model selection and estimate model parameters from the best-fitting models, applying a generalized linear model (GLM) regression procedure (8). We retained the 1,000 simulations with the smallest Euclidean distance from the observed data, and Bayes factors in support of the two models in the model selections approach (decline vs. expand) were calculated as the ratio of the marginal densities. We validated the ABC results by examining the coverage properties of

the posterior distribution, as recommended by Wegmann et al. (10). We obtained 1,000 pseudo-observed datasets from the simulations themselves and checked the distribution of the posterior quantiles for uniformity with a Kolmogorov–Smirnov test. In addition, we performed multiple regressions of the summary statistics against the model parameters to evaluate the information content of the chosen statistics with regard to the model parameters (11).

The heterochronous data allowed us to estimate two parameters of the microsatellite mutation model through the ABC analyses: the mutation rate (μ) and the shape parameter (p) of the geometric distribution of the General Stepwise Model. We estimated μ to be low, with a mean of 5.1×10^{-5} per generation, and p to be high with a mean of 0.82 (both values under the free model) (Table 3), which means that a high proportion of mutation events involved the addition or subtraction of several repeat units. Such parameters of a microsatellite mutation model can rarely be directly estimated from the data at hand but instead have to be incorporated according to standard values identified for completely different species and markers.

Estimating Population Census Size (N_c) for *D. robustus* Based on Genetic Data. Our best estimate of the effective population size (N_e) for *D. robustus* was ~9,200 individuals, which was the modal value taken from the free-model ABC analysis (Table 2). The conversion from N_e to the census population size (N_c) is not straightforward, but in this study we applied a 0.4 N_e/N_c ratio. The value represents the average of 20 estimated ratios for birds, as listed in Frankham (12). Here we discuss why this value also seems appropriate for *D. robustus*.

The ABC analyses showed that there were ~9,200 breeding *D. robustus* individuals at the time of human arrival. The analyses also demonstrated that there were equal numbers of breeding males and females in the population, yielding ~4,600 breeders of each sex. The fossil record shows that females outnumbered males among adults, and it has been argued that the 1:2.2 (male: female) ratio observed at Bell Hill Vineyard is the least biased estimate of sex ratios in moa (13). Because males were outnumbered, it seems reasonable to assume that there was female mating competition and that almost all males in the population would have bred (i.e., $N_e/N_c = 1$ for adult males). Using this rationale, we can estimate the census size for adult females to be 10,120 individuals (4,600 male $N_c \times 2.2$), thus giving a total of 14,720 adult *D. robustus* (4,600 males + 10,120 females).

The Bell Hill Vineyard collection includes 59% adult and 41% juvenile moa ($n = 120$; ref. 13). That this is a good estimate for a ratite population is supported by the observation of 64% adults among southern cassowaries (a forest-dwelling ratite and hence probably the closest ecological analog to moa) near Mission Beach, north Queensland (14). Assuming that 59% of giant moa individuals were adults, we estimated that the total standing census population for *D. robustus* to be 14,720/0.59 = 24,949 individuals at the time of Polynesia settlement. Based on these numbers, the overall N_e/N_c is then 9,200/24,949 ≈ 0.4, which is also the average for 20 bird species estimated previously (12).

Population Census Size (N_c) Estimate for *D. robustus* Based on Carrying Capacity of Different Ecological Regions. The ecologically based estimate of 158,000 moa in Holdaway and Jacomb (3) was for all species, in both islands, with 5% added to ensure a conservative result. The estimate for giant moa (which then included *D. giganteus*, *D. novaezealandiae*, and *D. struthoides*) was 45,272, again for both main islands. The South Island total was 23,974 giant moa (Dataset S2). That number now has to be revised as a result of the changes in giant moa taxonomy (15) and the availability of a much finer-grained description of the New Zealand terrestrial environments (16, 17) than the six-region model used by Holdaway and Jacomb (3). A single *Dinornis* species—*D. robustus*—is now recognized in the South Island (15). We present here a revised estimate for *D. robustus*, for comparison with the genetically based population size estimates (Dataset S3).

Leathwick et al. (16, 17) used nested categories based on a variety of climatic, topographic, and soil parameters. We used their level III as being areas recognized by the most appropriate combination of factors (primarily soil fertility, base material, slope, and annual temperature) to match the three levels of biomass carrying capacity used by Anderson (18) and Holdaway and Jacomb (3). Areas for each level III category are listed in Leathwick et al. (16). Carrying capacities in regions categorized as "steep hills" and "steep mountains" were taken to be one-third and one-sixth of the relevant carrying capacity based on soil fertility, because only fractions of the area would have been available to moa. Large ratites such as the dwarf cassowary (*Casuarius bennetti*) occupy only areas with moderate slope such as ridge tops in very steep terrain (19). In our model, males and females were taken to occupy separate, overlapping territories as has been shown for one of the only surviving obligate forest ratites, the southern cassowary (*Casuarius casuarius johnsonii*) (14). We assumed that females outnumbered males by the 1:2.2 ratio, as identified in the Bell Hill Vineyard fossil deposit and suggested to be the least biased estimate of sex ratios in adult moa (13).

Again applying Anderson's (18) methodology, we assigned one of the carrying capacities (best, 16.8 kg·km^{-2}; medium, 9.1 kg·km^{-2}; worst, 2.5 kg·km^{-2}) derived from work on emu (*Dromaius novaehollandiae*) to each of the level III land environments identified by Leathwick et al. (16, 17). We then calculated the number of individual male and female giant moa that each area could support, separately for males and females using the 1: 2.2 ratio as above, and average body masses of 200 and 100 kg for females and males, respectively (Dataset S3). *D. robustus* body mass varied with local climate, but individuals of all sizes occurred in every region (e.g., ref. 20). By using this methodology, the South Island total for territorial adults of both sexes was 8,296 individuals. By using the 59% adults (as explained above), the total population of *D. robustus* in the South Island would have been 8,296/0.59 = 14,061 (which we rounded to 14,100 in *Discussion*, *Population Size of* D. robustus). This value is 59% of the number calculated by using the six broad land environment areas. However, given the greater detail in habitat description and the more precise areas of each, in combination with a better understanding of the taxonomy and sex ratio of the bird, this value is likely to be a better estimate of the population of *D. robustus* in the South Island in the late Holocene.

Both the Holdaway and Jacomb (3) and our estimates are obviously broad brush. The earlier estimates were deliberately maximized to provide limiting conditions for modeling the effects of cropping rates (3). However, these estimates based on ecological factors do provide a basis for comparison with the estimates based on genetics, as they have done for modeling the effects of exploitation and habitat loss (3, 18). Ongoing work indicates that most moa taxa were confined to specific habitats within each ecological region, and population estimates based on carrying capacity and use of space will be refined further as the ecologies and microdistributions of taxa are better understood.

1. Bunce M, et al. (2009) The evolutionary history of the extinct ratite moa and New Zealand Neogene paleogeography. *Proc Natl Acad Sci USA* 106(49):20646–20651.
2. Gemmell NJ, Schwartz MK, Robertson BC (2004) Moa were many. *Proc Biol Sci* 271(Suppl 6):S430–S432.
3. Holdaway RN, Jacomb C (2000) Rapid extinction of the moas (Aves: Dinornithiformes): Model, test, and implications. *Science* 287(5461):2250–2254.
4. Rambaut A, Drummond A (2007) Tracer. Available at http://beast.bio.ed.ac.uk/Tracer. Accessed August 7, 2013.

5. Drummond AJ, Rambaut A (2007) BEAST: Bayesian evolutionary analysis by sampling trees. *BMC Evol Biol* 7(214):214.
6. Drummond A, Ho SYW, Rawlence NJ, Rambaut A (2007) A rough guide to BEAST 1.4 (Department of Computer Science, The University of Auckland, Auckland).
7. Rambaut A, Ho SYW, Drummond AJ, Shapiro B (2009) Accommodating the effect of ancient DNA damage on inferences of demographic histories. *Mol Biol Evol* 26(2): 245–248.
8. Wegmann D, Leuenberger C, Neuenschwander S, Excoffier L (2010) ABCtoolbox: a versatile toolkit for approximate Bayesian computations. *BMC Bioinformatics* 11:116.
9. Beaumont MA, Zhang W, Balding DJ (2002) Approximate Bayesian Computation in Population Genetics. *Genetics* 162:2025–2035.
10. Wegmann D, Leuenberger C, Excoffier L (2009) Efficient Approximate Bayesian Computation coupled with Markov Chain Monte Carlo without likelihood. *Genetics* 182:1207–1218.
11. Neuenschwander B, Branson M, Gsponer T (2008) Critical aspects of the Bayesian approach to phase I cancer trials. *Stat Med* 27(13):2420–2439.
12. Frankham R (1995) Effective population size/adult population size ratios in wildlife: A review. *Genet Res* 66(2):95–107.
13. Allentoft ME, Bunce M, Scofield RP, Hale ML, Holdaway RN (2010) Highly skewed sex ratios and biased fossil deposition of moa: Ancient DNA provides new insight on New Zealand's extinct megafauna. *Quat Sci Rev* 29(5-6):753–762.
14. Moore LA (2007) Population ecology of the southern cassowary *Casuarius casuarius johnsonii*, Mission Beach north Queensland. *J Ornithol* 148(3):357–366.
15. Bunce M, et al. (2003) Extreme reversed sexual size dimorphism in the extinct New Zealand moa Dinornis. *Nature* 425(6954):172–175.
16. Leathwick JR, et al. (2002) *Land Environments of New Zealand (Nga Taiao o Aotearoa): Technical Guide* (Ministry for the Environment, Wellington, New Zealand).
17. Leathwick JR, et al. (2003) *Land Environments of New Zealand. Nga Taiao o Aotearoa* (David Bateman, Auckland), p 184.
18. Anderson A (1989) Mechanics of overkill in the extinction of New-Zealand moas. *J Archaeol Sci* 16(2):137–151.
19. Mack AL (1995) Distance and nonrandomness of seed dispersal by the dwarf cassowary Casuarius-Bennetti. *Ecography* 18(3):286–295.
20. Worthy TH, Holdaway RN (2002) *The Lost World of the Moa* (Canterbury Univ Press, Christchurch, New Zealand), p 718.

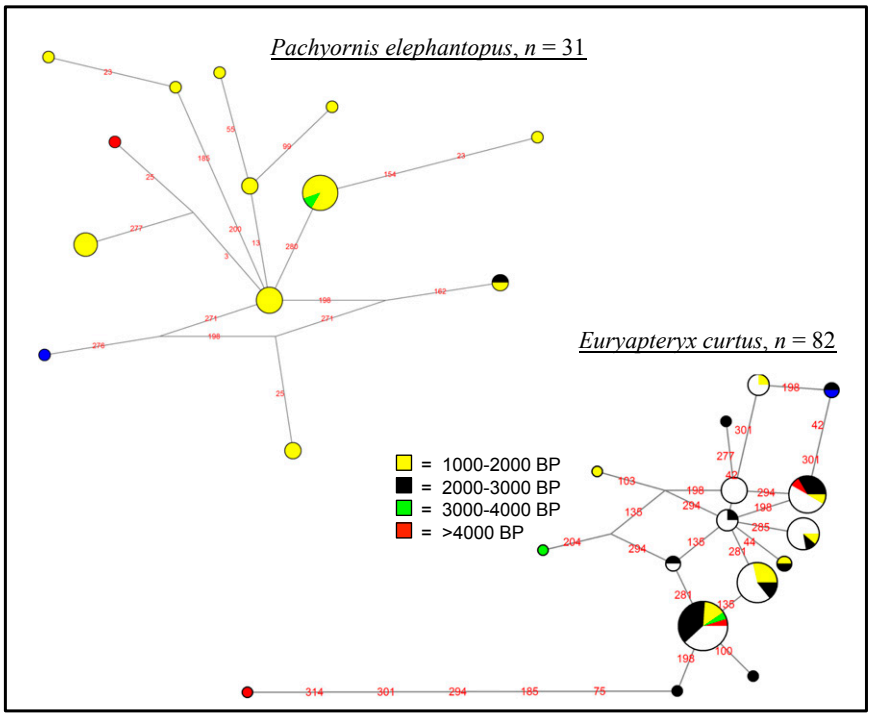

Fig. S1. Haplotype networks for *E. curtus* and *P. elephantopus* generated in NETWORK (Version 4.5) based on the ~340 bp of the mtDNA control region. Colors correspond to calibrated radiocarbon ages. Networks for *D. robustus* and *E. crassus* are shown in Fig. 2.

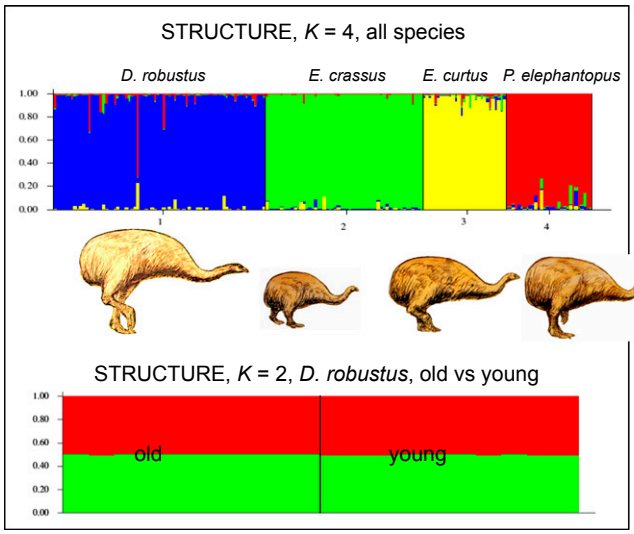

Fig. S2. STRUCTURE outputs. Bar plot outputs for the STRUCTURE analysis are shown. *Upper* shows the output for $K = 4$, where the genetic clustering is clearly defined by the four moa species. All intraspecific analyses, however, gave no signal of genetic structures. To illustrate that, *Lower* shows the STRUCTURE output based on a manipulated dataset for *D. robustus*, where only data from the 10 oldest and 10 youngest individuals were retained for analyses. The two temporal groups covered 4837–3270 B.P. and 602–1043 B.P., respectively, leaving a 2,200-y gap for genetic changes to have occurred. However, no genetic structuring is evident, indicating very limited effects of genetic drift exerted on the gene pools. The same pattern was evident for all four species.

Table S1. Tests for Hardy–Weinberg proportions

		MS2		MA1		MA21		MA38		MA44		MA46		Overall	
Taxon	*n*	F_{IS}	*P*	F_{IS}	*P*	F_{IS}	*P*	F_{IS}	*P*	F_{IS}	*P*	F_{IS}	*P*	F_{IS}	*P* (Fisher)
D. robustus	74	0.027	0.67	−0.010	0.9	**0.116**	**0.040**	0.061	0.33	0.080	0.257	0.010	0.24	0.040	0.227
P. elephantopus	30	0.191	0.39	**0.287**	**0**	−0.150	0.58	−0.018	0.64	−0.036	1	0.046	0.44	0.041	0.118
E. curtus	29	−0.043	0.82	−0.069	1	0.037	0.17	−0.129	0.91	−0.018	1	−0.146	1	−0.079	0.981
E. crassus	55	NA	NA	−0.031	1	−0.035	0.28	−0.089	0.78	NA	NA	NA	NA	−0.048	0.807

Fixation index (F_{IS}) and tests for Hardy–Weinberg proportions in the four moa populations. F_{IS} was calculated according to Weir and Cockerham (1), and the *P* value for each locus–taxon deviation was assessed with the exact test implemented in GENEPOP (Version 4.0.10; Rousset; ref. 2). Overall *P* value within each taxon was calculated by using Fisher's approach for combining probabilities. Values in boldface represent significant deviations ($\alpha = 0.05$). NA represents monomorphic or nearly monomorphic loci.

1. Weir BS, Cockerham CC (1984) Estimating F-statistics for the analysis of population structure. *Evolution* 38(6):1358–1370.
2. Rousset F (2008) genepop'007: A complete re-implementation of the genepop software for Windows and Linux. *Mol Ecol Resour* 8(1):103–106.

Table S2. F_{ST} between individuals at different times

Age group	*n*	<1,000 B.P.	1,000–2,000 B.P.	2,001–3,000 B.P.	>3,000 B.P.
<1,000 B.P.	8	—	0.26	0.23	0.22
1,000–2,000 B.P.	36	0.004	—	0.36	0.44
2,001–3,000 B.P.	20	0.013	0.001	—	0.10
>3,000 B.P.	10	0.028	0.000	0.012	—

Pairwise F_{ST} values (lower half) between the four different age groups in *D. robustus*, and *P* values (upper half) calculated as the fraction of 6,000 randomizations resulting in same or higher F_{ST} values than the observed.

Table S3. BEAST scenarios and results

	Growth rate		Onset of demographic change, y B.P.		Effective female *Ne*		
Model	Prior	Posterior	Prior	Posterior	Prior	Posterior	Ln likelihood
BSP	NA	NA	NA	~13,000*	10,000 (no bound)	20,000 (1,900; 44,700)	−747
Constant	NA	NA	NA	NA	10,000 (no bound)	13,200 (1,700; 37,000)	−741
Free model	0 (-0.01; 0.01)	2.3E-4 (4.7E-8; 4.5E-4)	10,000 (500; 30,000)	18,800 (11,800; 26,500)	10,000 (0; 5E5)	14,600 (1,900; 36,200)	−749
Model selection: expand	0 (0.00; 0.01)	2.3E-4 (1.6E-7; 4.6E-4)	10,000 (500; 30,000)	18,600 (11,900; 26,600)	10,000 (0; 5E5)	14,700 (1,900; 36,500)	−750
Model selection: decline	0 (-0.01; 0.00)	NA	10,000 (500; 30,000)	NA	10,000 (0; 5E5)	NA	*-infinity*

Prior settings and posterior result for the models explored in BEAST using the *D. robustus* mtDNA data. BSP is the Bayesian skyline model with no restrictions on either growth rate or the timing of a demographic change. Further, we tested a constant population size model and three single-change-point models, including the free model, which allows both positive and negative growth rates, whereas the expand and decline models were restricted to positive and negative growth, respectively. Marginal likelihood (estimated with 1,000 bootstraps in TRACER) is highest for the constant model, implying that we cannot reject a constant population size. However, the BSP signal indicates a weak population increase during the mid- to late Holocene (Fig. 3), and the population decline model is deemed extremely unlikely, with *-infinity* likelihood values. All depicted priors were run with a uniform distribution: start (minimum; maximum). Posteriors display mean value and 95% HPDs, where applicable. The effective female population size (N_e) was calculated based on a 10 y generation time (Rawlence et al.; ref. 1).
*See Fig. 3.

1.Rawlence NJ, et al. (2012) The effect of climate and environmental change on the megafaunal moa of New Zealand in the absence of humans. *Quaternary Science Reviews* 50:141–153.

Table S4. ABC marginal densities

Model	Marginal density	*P* value
Free model	**0.31**	**0.995**
Model selection: decline	0.24	0.998
Model selection: expand	**1.26**	**0.996**

Marginal densities of models. Parameters were estimated and validation was carried out for the models marked in bold (Table 3 and Table S5). *P* values correspond to the proportion of retained simulations that have a lower likelihood than the observed data under the ABC-inferred GLM and hence estimates the probability of obtaining the observed values under a given scenario. Among the two directly comparable models in the model selection approach (decline vs. expand), the Bayes factor was 5.25, indicating substantial support for the *expand* model (Jeffreys; ref. 1).

1. Jeffreys H (1961) *The Theory of Probability* (Oxford Univ Press, Oxford), 3rd Ed.

Table S5. ABC summary statistics

Dataset	Summary statistic
Microsatellites	
Bin 1	Heterozygosity
Bin 1	No. of alleles
Bin 1	Garza–Williamson index
Bin 1	Allelic range
Bin 2	Heterozygosity
Bin 2	No. of alleles
Bin 2	Garza–Williamson index
Bin 2	Allelic range
Combined	Heterozygosity
Combined	No. of alleles
Combined	Allelic range
Among	F_{ST}
mtDNA	
Bin 1	No. of haplotypes
Bin 1	Nucleotide diversity
Bin 1	Tajima's D
Bin 2	No. of haplotypes
Bin 2	Nucleotide diversity
Bin 2	Tajima's D
Combined	No. of haplotypes

The list of 19 summary statistics used in the ABC analyses of the *D. robustus* data. The statistics were calculated in and across each of two age bins of equal sample size (n = 37), divided at 1320 y B.P. (calibrated).

Other Supporting Information Files

Dataset S1 (XLSX)
Dataset S2 (PDF)
Dataset S3 (PDF)